Journal of Solid State Chemistry 183 (2010) 1388–1393

Contents lists available at ScienceDirect

Journal of Solid State Chemistry

journal homepage: www.elsevier.com/locate/jssc

Lattice crossover and mixed valency in the $LaCo_{1-x}Rh_xO_3$ solid solution

Jun Li [a], Andrew E. Smith [a], Kyei-Sing Kwong [b], Cynthia Powell [b], Arthur W. Sleight [a], M.A. Subramanian [a,*]

[a] Department of Chemistry, Oregon State University, Corvallis, OR 97331-4003, USA
[b] National Energy Technology Laboratory-Albany, US DOE, Albany, OR 97321, USA

ARTICLE INFO

Article history:
Received 6 February 2010
Received in revised form
12 April 2010
Accepted 14 April 2010
Available online 18 April 2010

Keywords:
Cobalt oxides
Rhodium oxides
Perovskites
Solid solutions
Thermoelectrics
Magnetism

ABSTRACT

The full $LaCo_{1-x}Rh_xO_3$ solid solution was investigated utilizing structural, electrical transport, magnetic, and thermal conductivity characterization. Strong evidence for at least some conversion of Rh^{3+}/Co^{3+} to Rh^{4+}/Co^{2+} is found in both structural and electrical transport data. The crystal structure is that of a rhombohedrally distorted perovskite over the range $0.0 \le x \le 0.1$. The common orthorhombic distortion of the perovskite structure is found over the range $0.2 \le x \le 1.0$. A crossover of all three orthorhombic cell edges occurs at $x=0.5$ giving the appearance of a cubic structure, which actually remains orthorhombic. The octahedra in the orthorhombic structure must be distorted for x values less than 0.5, and the observed distortion suggests orbital ordering for Co^{2+}. Electrical resistivity measurements as a function of temperature show semiconducting-like regions for all compositions. There is a steady increase in electrical resistivity as the Rh content increases. Large positive thermopower values are generally obtained above 475 K. With increasing Rh substitution there is a decrease in thermal conductivity, which slowly rises with increasing temperature due to increased electrical conductivity. The electronic part of the thermal conductivity is suppressed significantly upon Rh substitution. A thermoelectric figure-of-merit (ZT) of about 0.075 has been achieved for $LaCo_{0.5}Rh_{0.5}O_3$ at 775 K, and is expected to reach 0.15 at 1000 K.

1. Introduction

A constraint in the ideal cubic AMO_3 perovskite structure is that the A–O bond distance must equal the M–O bond distance times $\sqrt{2}$. Thus, Goldschmidt defined a tolerance factor, t, as $t=(r_A+r_O)/[\sqrt{2}(r_M+r_O)]$, where r_A, r_M, and r_O are the radii of the A cation, M cation, and O anion, respectively [1]. The relative sizes of the A and M cations are such in most compounds with the perovskite structure that t is less than 1.0. Temperature impacts t because the A cations have higher thermal expansion than the M cations; thus, increasing temperature increases t. Reducing t from 1.0 results in distortions of the perovskite structure, which decrease the coordination number of the A cation. These distortions may be described as a tilting of the octahedra in the MO_3 network [2,3]. The most common tilt structure has orthorhombic symmetry, and this structure is found for many RMO_3 perovskites where R is a rare earth cation and t is less than about 0.985 [4,5]. As the size of R increases t increases, and a change occurs to a tilt structure with rhombohedral symmetry, and with increasing temperature the further increase in t results in a transformation to the ideal cubic structure [5]. However before the change from orthorhombic to rhombohedral occurs for the RMO_3 perovskites, there is a crossover of all three orthorhombic cell edges such that powder diffraction patterns appear to be cubic at the crossover point. This sequence observed for the RMO_3 perovskites is not universal for all AMX_3 compounds with the perovskite structure. For example, in the $Na_{1-x}K_xMgF_3$ solid solution with increasing x and t, there is no crossover of the orthorhombic cell edges, which ultimately convert to tetragonal and then cubic [6]. Increasing temperature for low x phases results in a smooth transition to the ideal cubic structure with no crossover and no structure of intermediate symmetry [7]. We have now observed dramatic crossover behavior with a change of the M cation as x is varied in the $LaCo_{1-x}Rh_xO_3$ solid solution.

Transition metal oxides with perovskite-type structures have been of interest for many years due to their great variety of observed properties, including very high dielectric constants, high T_c superconductivity, ferromagnetism, and useful catalytic behavior [8]. Little attention was given to oxides as potentially efficient thermoelectrics until good thermoelectric properties were found for some Co based oxides [9–13]. Subsequently, there has been an increased interest in the thermoelectric properties of perovskite oxides [14,15]. In general, oxides have an advantage over other thermoelectric materials, like bismuth chalcogenides, in that they are stable to far higher temperatures. Solid solutions of $LaCoO_3$ and $LaRhO_3$ have been studied for their electrical, magnetic, and catalytic properties [16–23]. However, the crystallographic, electrical and magnetic properties of the entire solid solution in

* Corresponding author. Tel.: +1 541 737 8235.
E-mail address: mas.subramanian@oregonstate.edu (M.A. Subramanian).

0022-4596/$ - see front matter © 2010 Elsevier Inc. All rights reserved.
doi:10.1016/j.jssc.2010.04.021

$LaCo_{1-x}Rh_xO_3$ have not been reported. Our goal was to investigate the structural variation and physical properties of the complete solid solution between $LaCoO_3$ and $LaRhO_3$.

2. Experimental

Polycrystalline samples of $LaCo_{1-x}Rh_xO_3$ ($x=0$–1) were synthesized using traditional solid state methods. Starting materials of La_2O_3 (Aldrich 99.9%), Co_3O_4 (Alfa Aesar 99%), and Rh_2O_3 were mixed thoroughly in appropriate ratios. Rh_2O_3 was obtained by the oxidation of RhI_3 (JMC 98%) in an oxygen gas flow at 700 °C for 12 h. La_2O_3 was dried at 850 °C overnight before weighing. The mixed powders of starting materials were calcined at 1200 °C for 12 h in air with ramp rates of 300 °C/h. The samples were reground and sintered twice in air at 1250 °C for 12 h with a ramp up rate of 150 °C/h and a ramp down rate of 100 °C/h. $LaRhO_3$ was prepared by heating at 1200 °C in an oxygen gas flow. The reacted powders were cold pressed before sintering. Powder X-ray diffraction data were collected with a Rigaku MiniFlex II powder diffractometer using Cu $K\alpha$ radiation and a graphite monochromator on the diffracted beam. The electrical resistivities and Seebeck coefficients were measured from 300 to 800 K by a standard four-probe technique with a ULVAC-ZEM themoanalyzer in a He atmosphere. The Seebeck coefficient was measured with constantan as a reference. The absolute uncertainty in both parameters is estimated to be below 5%. The thermal conductivity was determined using a Netzsch Laser Microflash with reference material of graphite-coated Pyroceram for diffusivity and the heat capacity was assumed to be that of $LaCoO_3$. The samples were measured without graphite coatings. Magnetism was measured with a PPMS Physical Property Measurement System with an EverCool He(l) recycling system from 5 to 300 K under an applied field of 0.5 T.

3. Results and discussion

3.1. Structural behavior

X-ray powder diffraction patterns of the compositions $LaCo_{1-x}Rh_xO_3$ ($x=0$–1) are shown in Fig. 1. With the increasing amount of Rh, a rhombohedral-to-orthorhombic transition occurs between x values of 0.1 and 0.2. This transition is evident from the change in the splittings of the pseudocubic peaks of the ideal perovskite structure and from the appearance and rise of new peaks such as the (111) reflection near 25.5° 2θ. The diffraction data were fitted by Rietveld refinements using the GSAS software suite [24,25]. A typical calculated profile is given for $LaCo_{1-x}Rh_xO_3$ ($x=0.5$) in Fig. S1. Unit cell parameters vs. composition are shown in Fig. 2. The b cell edge has been divided by $\sqrt{2}$ because this would then have the same value as a and c, if the structure were the ideal cubic perovskite structure (Fig. 2(a)). The unit cell volume (V) vs. composition and $V^{1/3}$ vs. composition are shown in Fig. 2(b). Végard's Law would have a linear relationship for $V^{1/3}$ vs. composition, but it is generally found that V vs. composition is more likely to be linear [26]. Either way the volume plot shows a positive deviation. The α angle for rhombohedral phases increases from 60.8° for $x=0$ to 61.0° for $x=0.1$ showing a slightly increased rhombohedral distortion with increasing Rh concentration. The possibility of ordering of Co and Rh on the octahedral sites was considered and was found not to occur for any value of x.

The continuous solid solution of $LaCo_{1-x}Rh_xO_3$ ($x=0.2$–0.9) is found to be isostructural with perovskite $LaRhO_3$ [27]. The structure for this very common orthorhombic distortion of the cubic perovskite is described in space group #62. There are six different settings for this space group, each with its unique space group designation. The two most commonly used designations are *Pnma* and *Pbnm*. We have chosen to use the *Pnma* setting for the orthorhombic $LaCo_{1-x}Rh_xO_3$ phases. The cell volume increases as expected when replacing Co with larger Rh ions in the $LaCoO_3$ structure (Fig. 2(b)), mainly a result of the lattice

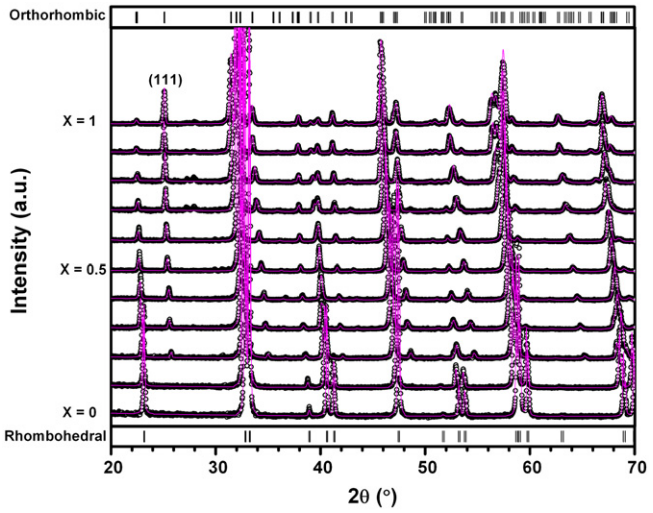

Fig. 1. XRD patterns of $LaCo_{1-x}Rh_xO_3$ (open circles) and calculated data (solid line) by Rietveld refinement. Allowed Bragg reflections are shown as vertical lines for both structural variations.

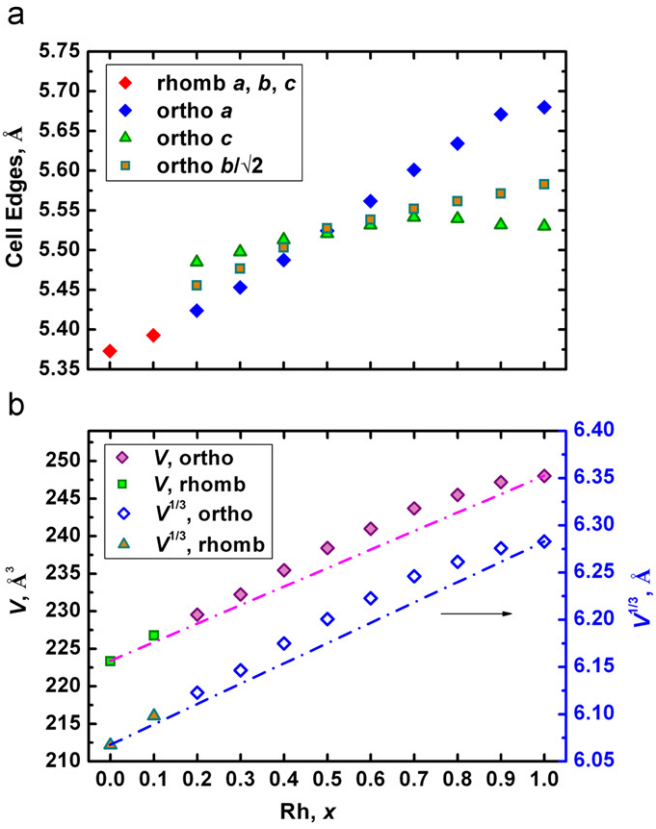

Fig. 2. Cell parameters as a function of Rh concentration for solid solutions $LaCo_{1-x}Rh_xO_3$. Straight lines are drawn to guide the eyes. (a) Cell edge b of the orthorhombic phase was divided by $\sqrt{2}$; (b) cell volume V of the rhombohedral phase was normalized ($\times 2$), based on Z, to match the orthorhombic cell volume.

expansion of the *a* cell edge. The *c* cell edge remains almost unchanged. The refined site occupancies for Rh are in good agreement with the intended substitution levels. Detailed crystallographic results for $LaCo_{1-x}Rh_xO_3$ are available in Tables S1 and S2. The correctness of our assignments of the *a* and *c* axes was verified by comparison with refinements where *a* and *c* were interchanged.

The most common perovskite tilt structure is the orthorhombic structure that we describe in the *Pnma* space group [4]. However, this tilt structure normally converts to a tilt structure of higher symmetry with increasing *t* before finally converting to the ideal cubic structure with no tilting. For RMO_3 phases where *R* is a trivalent rare earth cation, the *Pnma* orthorhombic structure transforms to a rhombohedral tilt structure with increasing *t* [5,28]. Such behavior occurs for *M*=Co, Ni, and Al as the size of the rare earth cation increases [5]. However before the transformation to rhombohedral, there is a crossover of the cell edges of the orthorhombic phase such that $a=c=b/\sqrt{2}$ at the crossover point. The diffraction pattern at this point can be indexed as cubic even though the true symmetry remains orthorhombic. Tilting of ideal octahedra in *Pnma* necessarily results in $a>b/\sqrt{2}>c$. This is the order observed for the lower values of *t*, but after the crossover with increasing *t* the order becomes $a<b/\sqrt{2}<c$. This order can only be achieved through a distortion of the MO_6 octahedra, and a deviation of O–*M*–O angles of only 1° from 90° can account for the crossover [29].

The behavior that we observe for $LaCo_{1-x}Rh_xO_3$ phases with changing *x* is thus analogous to that reported for RMO_3 phases. As *x* for $LaCo_{1-x}Rh_xO_3$ phases decreases *t* increases, and there is first a crossover of the orthorhombic cell edges and then a transformation to a rhombohedral structure. SPuDS software calculates *t*, cell dimensions and tilt angles based on cation sizes and an assumed tilt structure with ideal octahedra [30]. These values calculated with SPuDS for the $LaCo_{1-x}Rh_xO_3$ solid solution are shown in Fig. 3. As expected, SPuDS predicts a monotonic decrease of cell edges with decreasing *x* and a smooth transition to cubic symmetry. It cannot predict the crossover because the crossover cannot occur for the ideal octahedra assumed by SPuDS. The observed crossover point for $LaCo_{1-x}Rh_xO_3$ occurs at *x*=0.5 where there are equal amounts of Rh and Co. The lattice strain caused by the orthorhombic distortion has become zero at the crossover point (Fig. S2). When the octahedra become distorted, there is no longer a precise definition of the tilt angle. However, using the equations of O'Keeffe and Hyde [31] the tilt angles (Fig. 3) were calculated from our refined O positions using Tubers software [30]. The slopes of the tilt angle vs. *x* curves are essentially the same from SPuDS and Tubers, but the values calculated from our refined structures are always somewhat higher.

An *x* value for the crossover of 0.5 might seem a mere coincidence, except that such behavior has been previously observed in the $La_{1-x}Sr_xRuO_3$ system [32]. The orthorhombic *Pnma* structure exists for all values of *x* in this system, but there is a crossover at *x*=0.5 where there are equal amounts of La and Sr and of Ru^{3+} and Ru^{4+}. This suggests the possibility that the crossover point of *x*=0.5 in both systems is not accidental and merits a more intensive study. The value of *t* is the same at the crossover point for both $LaCo_{1-x}Rh_xO_3$ and $La_{1-x}Sr_xRuO_3$, 0.96 as calculated by SPuDS. However, the crossover point for the $RNiO_3$ series is found for $NdNiO_3$ where the value of *t* is 0.92 as calculated by SPuDS [5].

Bond distances and bond angles vs. composition for $LaCo_{1-x}Rh_xO_3$ phases are shown in Figs. 4 and 5. We know that the MO_6 octahedra must be distorted on the Co rich side of the crossover, but some distortion is also expected on the Rh rich side because such distortion has been reported for $LaRhO_3$ [27]. We observe an increase in octahedral distortion with decreasing *x* and

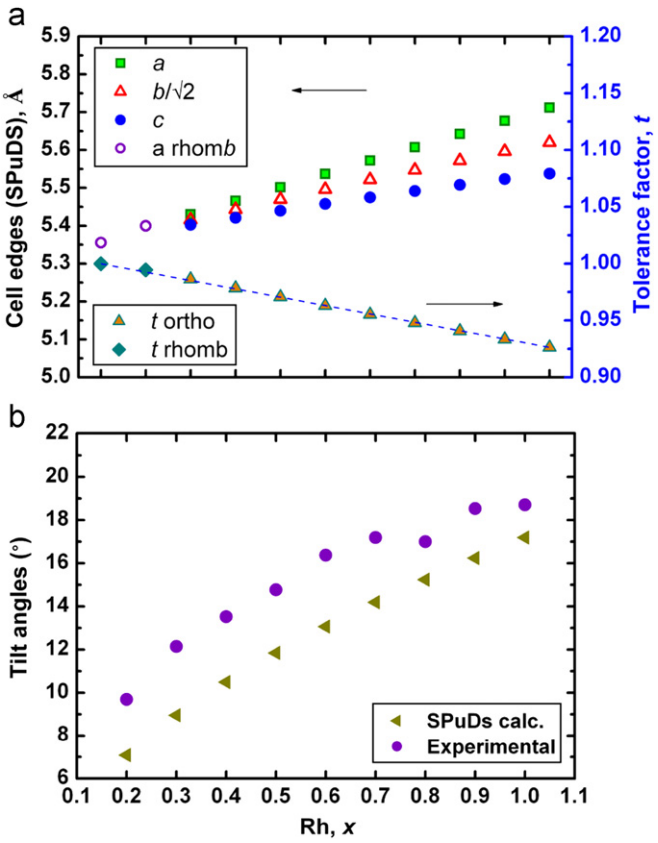

Fig. 3. Cell edges and tolerance factor *t* calculated by SPuDS (a), and observed and predicted tilt angles calculated by Tubers and SPuDS, respectively, (b).

increasing *t*, and the distortion becomes more pronounced with regard to both bond angles and *M*–O distances on the Co rich side of the crossover. The shorter *M*–O distance along the *b* axis at *x*=0.2 is suggestive of orbital ordering for Co^{2+}, but further studies would be required to establish this. We cannot assume that the oxidation states of Co and Rh are +3 in the solid solution. In the case of the $LaCo^{3+}O_3$–$CaRu^{4+}O_3$ solid solution, the oxidation states are Co^{2+} and Ru^{5+} for the composition $LaCaCoRuO_6$ [33]. Furthermore, evidence is found at this composition for orbital ordering for Co^{2+}. The electronic configuration of $t_{2g}^5e_g^2$ for high spin Co^{2+} favors a tetragonal distortion of an octahedron to produce 4 long and 2 short *M*–O distances, as observed in $LaCaCoRuO_6$ and apparently also at low *x* values in orthorhombic $LaCo_{1-x}Rh_xO_3$ phases. No configuration of Co^{3+} is expected to give such a distortion. This distortion of the octahedra is facilitated in the low *x* orthorhombic $LaCo_{1-x}Rh_xO_3$ phases because the octahedron must be distorted on that side of the crossover.

3.2. Electrical properties

Both Rh^{3+} and Co^{3+} are d^6 cations. For Rh^{3+} oxides the low spin state always pertains due to the gap of about 2.2 eV between the t_{2g} and e_g bands. Thus, Rh^{3+} oxides are insulating with room temperature resistivities higher than $10^6\,\Omega$ cm unless they are doped, which may be inadvertent [34]. Doping or nonstoichiometry can lead to holes in the t_{2g} band or electrons in the e_g band, thus giving either p-type or n-type conductivity. The gap between the t_{2g} and e_g bands in Co^{3+} oxides is much less than for Rh^{3+} oxides. At the lowest temperatures all of the 3*d* electrons for $LaCoO_3$ are in the t_{2g} levels, which are filled giving low spin Co^{3+}. The gap to the e_g levels is so small that electrons from the t_{2g}

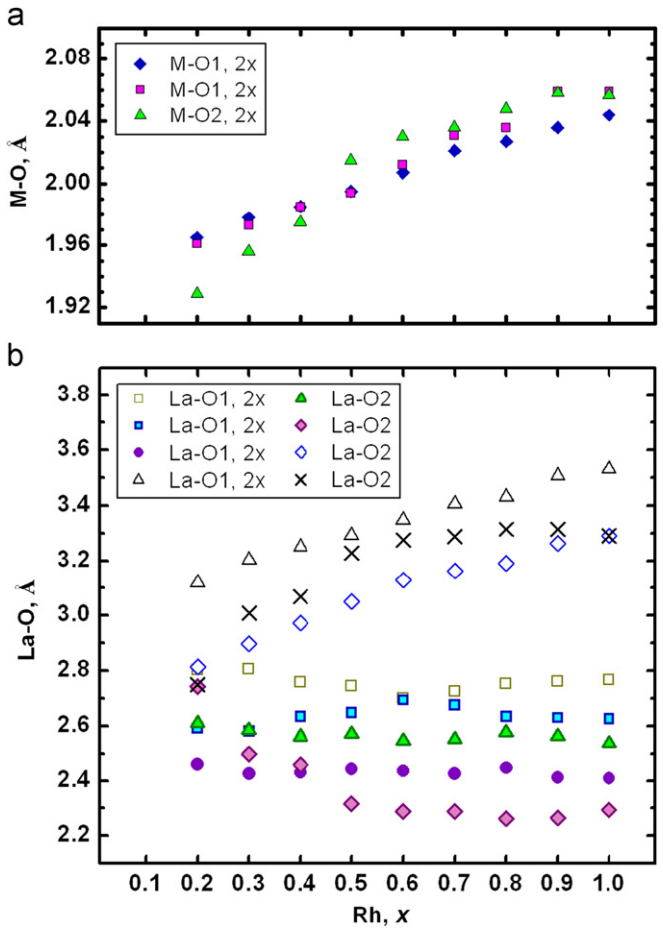

Fig. 4. Bond distances vs. x in $LaCo_{1-x}Rh_xO_3$.

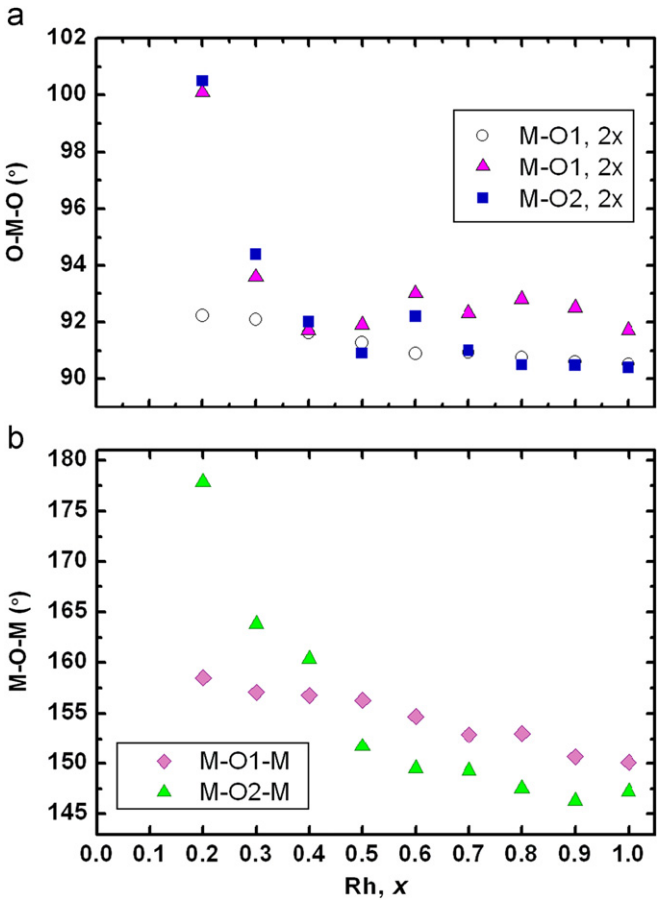

Fig. 5. Bond angles vs. x in $LaCo_{1-x}Rh_xO_3$.

levels are excited into these levels with increasing temperature [35]. On reaching 640 K there are equal amounts of low spin and high spin Co^{3+}. The excitations of electrons from t_{2g} to e_g levels do not necessarily occur on the same Co atom. Thus, this excitation creates some Co^{2+} and Co^{4+}, and this is believed to be an important aspect of the conduction process in $LaCoO_3$ [35]. As Rh is substituted for Co we see an increase in resistivity due to the dilution of the 3d electrons (Fig. 6).

The situation is much simpler on the Rh rich end of the $LaCo_{1-x}Rh_xO_3$ solid solution. The observed electrical conductivity for $x=1.0$ (Fig. 6) is due to holes in the Rh 4d t_{2g} band. The drop in both resistivity and Seebeck coefficient is most pronounced for the first 10% replacement of Co for Rh, especially noticeable at higher temperatures (Fig. 6). The increase in conductivity with the 10% Co substitution indicates that Co is an effective p-type dopant for $LaRhO_3$. This is equivalent to the conversion of Rh^{3+}/Co^{3+} to Rh^{4+}/Co^{2+}. The positive deviation from linearity of the unit cell volume vs. composition plot (Fig. 2(b)) can now be explained because a Rh^{4+}/Co^{2+} combination occupies more space than a Rh^{3+}/Co^{3+} combination. The radius sum for Rh^{4+}/Co^{2+} is 1.35 Å compared to a radius sum for Rh^{3+}/Co^{3+} of 1.21 or 1.27 Å, depending on whether Co^{3+} is low spin or high spin [36]. The positive deviation in Fig. 2(b) suggests that some conversion of Rh^{3+}/Co^{3+} to Rh^{4+}/Co^{2+} occurs over the entire range where both Co and Rh are present. This is thus a very complicated region where Rh^{3+}, Rh^{4+}, Co^{2+}, Co^{3+}(low-spin), and Co^{3+}(high-spin) are all present, and their relative amounts are likely changing with temperature.

The Seebeck coefficient behavior we find for $LaCoO_3$ with a crossover from negative to positive values at about 450 K is similar to that reported by He et al. [16]. With increasing Rh substitution and increasing resistivity, the Seebeck coefficient (Fig. 6) also increases.

The temperature dependence of thermal conductivity and ZT for $LaCo_{1-x}Rh_xO_3$ ($x=0$–0.5) phases are shown in Fig. 7. The thermal conductivity of $LaCoO_3$ reported here is consistent with previous reports [16,37,38]. Substitution of Rh for Co decreases the thermal conductivity dramatically. Using the Wiedmann-Franz law, $\kappa=L_0T/\rho$ (where $L_0=2.44\times10^{-8}\,V^2/K^2$) and our experimental results, the electronic contribution to the thermal conductivity was calculated for $LaCoO_3$ (~13% at ~520 K) and $LaCo_{1-x}Rh_xO_3$ where $x=0.1$–0.5 (9.5%, 6.5%, 4%, 2.5%, 2%, respectively, at 520 K). The electronic contribution to the thermal conductivity increases with increase in temperature. Thus, the lattice thermal conductivity is important and the introduction of Rh suppresses the electronic contribution to the total thermal conductivity. This reduction may be attributed to increased phonon scattering due to the lattice disruption caused by having Rh^{3+}, Rh^{4+}, Co^{2+}, Co^{3+}(low-spin), and Co^{3+}(high-spin) all occupying the octahedral sites. The large changes in the thermopower, resistivity, and thermal conductivity occur consistently in the same temperature range. An increase in the ZT occurs in $LaCo_{1-x}Rh_xO_3$ phases as x increases to 0.5 (Fig. 7). In all cases ZT increases with increase in temperature. A ZT of ~0.075 is obtained for $LaCo_{0.5}Rh_{0.5}O_3$ at 775 K. It is expected that the ZT of this sample may reach as high as 0.15 at $T=1000$ K based on best fit approximations.

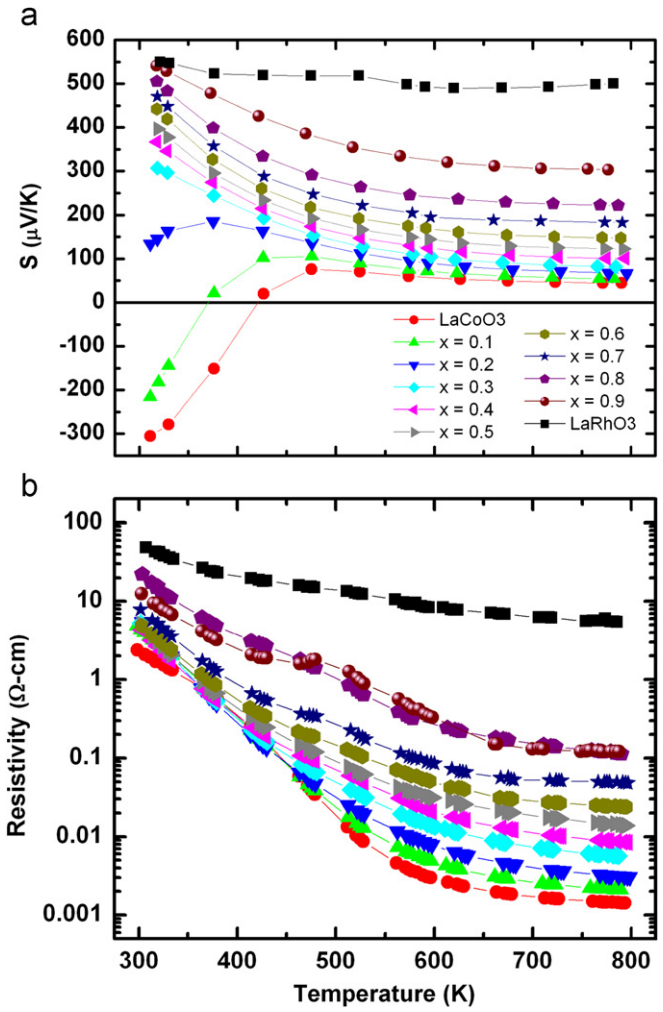

Fig. 6. Temperature dependence of the Seebeck coefficients (a) and electrical resistivity (b) for $LaCo_{1-x}Rh_xO_3$.

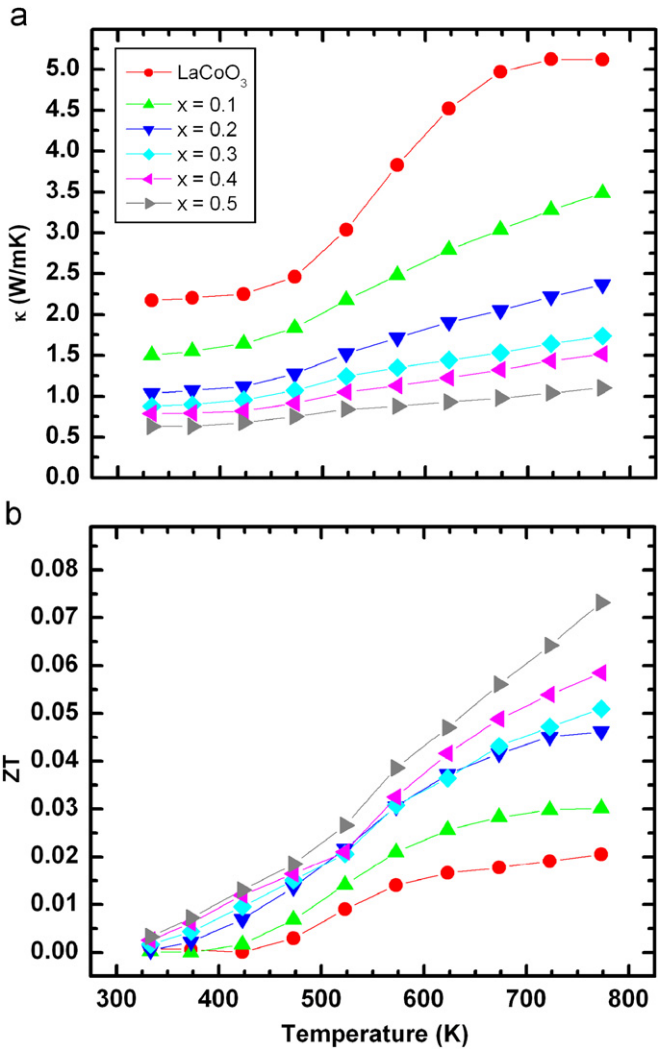

Fig. 7. Temperature dependence of the thermal conductivity (a) and dimensionless figure-of-merit ZT (b) for $LaCo_{1-x}Rh_xO_3$.

3.3. *Magnetic properties*

The magnetic properties of $LaCoO_3$ have been previously investigated by many groups. The $1/\chi$ vs. T plot (Fig. S3) for $LaCoO_3$ might suggest Curie–Weiss behavior above ~150 K. However, we know that there is actually no temperature region of Curie–Weiss behavior for $LaCoO_3$. This is because the relative amount of high spin Co^{3+} is steadily increases with increase in temperature. The situation becomes even more complex in the $LaCo_{1-x}Rh_xO_3$ solid solution because Rh^{3+}, Rh^{4+}, Co^{2+}, Co^{3+}(low-spin), and Co^{3+}(high-spin) are all present, and the relative amounts of these species are likely temperature dependent at each composition. Thus, an interpretation of the plots as Curie–Weiss behavior is not possible.

4. Conclusions

We have no explanation as to why crossover of lattice parameters occurs in both the $LaCo_{1-x}Rh_xO_3$ and $La_{1-x}Sr_xRuO_3$ systems at $x=0.5$, and perhaps this is accidental. It is, however, the value of x where charge ordering is most likely to occur. Charge ordering of Ru^{3+} and Ru^{4+} might seem a possibility in the $La_{1-x}Sr_xRuO_3$ system, but this will be impeded by the disorder of La and Sr on the *A* sites and by the delocalized nature of the 4*d* electrons of Ru. Likewise, charge order would be very difficult in the $LaCo_{1-x}Rh_xO_3$ system considering the likely simultaneous presence of Rh^{3+}, Rh^{4+}, Co^{2+}, Co^{3+}(low-spin), and Co^{3+}(high-spin) species. Furthermore, it is not obvious how charge ordering might relate to the crossover. There are no reported structure refinements near the crossover for the $La_{1-x}Sr_xRuO_3$ system, and our structure refinements in the $LaCo_{1-x}Rh_xO_3$ system are not very accurate. We plan to refine structures close to the crossover point in both systems using neutron diffraction data. This should also help define whether there is a good basis for orbital ordering for Co^{2+}. Although there is reason to believe that some conversion of Rh^{3+}/Co^{3+} to Rh^{4+}/Co^{2+} occurs in the $LaCo_{1-x}Rh_xO_3$ system, the degree to which this occurs is uncertain. Resolving this would be a very challenging spectroscopic study. Our transport measurements indicate that increasing rhodium in the $LaCo_{1-x}Rh_xO_3$ system improves thermoelectric properties.

Acknowledgments

This technical effort was performed in support of the NETL's on-going research on development of materials for energy applications under the RDS Contract DE-AC26-04NT41817. The work performed at Oregon State University was also supported by NSF Grant (DMR 0804167). A.E.S would like to thank NSF-IGERT for financial support.

Appendix A. Supplementary materials

Supplementary data associated with this article can be found in the online version at doi:10.1016/j.jssc.2010.04.021.

References

[1] V.M. Goldschmidt, Naturwissenschaften 14 (1926) 477.
[2] A.M. Glaser, Acta Cryst. B 28 (1972) 3384.
[3] P.M. Woodward, Acta Cryst. B 53 (1997) 32.
[4] P.M. Woodward, Acta Cryst. B 53 (1997) 44.
[5] P. Lacorre, J.B. Torance, J. Pannetier, A.I. Nazzal, P.W. Wang, Y.C. Huang, J. Solid State Chem. 91 (1991) 225.
[6] Y. Zhao, J. Solid State Chem. 141 (1998) 121.
[7] A. Yoshiasa, D. Sakamoto, H. Okudera, M. Ohkawa, K. Ota, Mater. Res. Bull. 38 (2003) 421.
[8] F.C. Galasso, Perovskites and High T_c Superconductors, Gordon and Breach Science Publishers, New York, 1990.
[9] I. Terasaki, N. Murayama (Eds.), Oxide Thermoelectrics, Research Signpost, Trivandrum, India, 2002.
[10] J. Androulakis, P. Migiakis, J. Giapintzakis, Appl. Phys. Lett. 84 (2004) 1099.
[11] Y. Wang, Y. Suia, J. Cheng, X. Wang, W. Su., J. Alloys Compd. 477 (2009) 817.
[12] K. Kurosaki, H. Muta, M. Uno, S. Yamanaka, J. Alloys Compd. 315 (2001) 234.
[13] T. Seetawan, V. Amornkitbamrung, T. Burinprakhon, S. Maensiri, K. Kurosaki, H. Mutab, M. Uno, S. Yamanaka, J. Alloys Compd. 407 (2006) 314.
[14] T.M. Tritt, M.A. Subramanian, Mater. Res. Soc. Bull. 31 (2006) 188.
[15] A.E. Smith, A.W. Sleight, M.A. Subramanian, Mater. Res. Bull. 45 (2010) 460.
[16] T. He, J. Chen, T.G. Calvarese, M.A. Subramanian, Solid State Sci. 8 (2006) 467.
[17] S. ShibasakiY. Takahashi, I. Terasaki, J. Electron. Mater. 38 (2009) 1013.
[18] S. Shibasaki, Y. Takahashi, I. Terasaki, J. Phys. Condens. Matter 21 (2009) 115501.
[19] M.A. Senaris-Rodriguez, J.B. Goodenough, J. Solid State Chem. 118 (1995) 323.
[20] M. Kriener, C. Zobel, A. Reichl, J. Baier, M. Cwik, K. Berggold, H. Kierspel, O. Zabara, A. Freimuth, T. Lorenz, Phys. Rev. B 69 (2004) 094417.
[21] T. Kyomen, Y. Asaka, M. Itoh, Phys. Rev. B 67 (2003) 144424.
[22] P.R. Watson, G.A. Somorjai, J. Catal. 74 (1982) 282.
[23] N.N. Lubinskii, L.A. Bashkirov, G.S. Petro, S.V. Schevchenko, I.N. Kandidatova, M.V. Bushinskii, Glass Ceram. 66 (2009) 59.
[24] A.C. Larson, R.B. Von Dreele, General Structure Analysis System (GSAS), Los Alamos National Laboratory Report LAUR 86–784, 2004.
[25] B.H. Toby, EXPGUI, a graphical user interface for GSAS, J. Appl. Cryst. 34 (2001) 210.
[26] K.A. Gschneiderner, G.H. Vineyard, J. Appl. Phys. 33 (1962) 3444.
[27] R.B. Macquart, M.D. Smith, H.C. zur Loye, Cryst. Growth Des. 6 (2006) 1361.
[28] J.-S. Zhou, J.B. Goodenough, Phys. Rev. Lett. 94 (2005) 065501.
[29] P.M. Woodward, T. Vogt, D.E. Cox, A. Arulraj, C.N.R. Rao, P. Karen, A.K. Cheetham, Chem. Mater. 10 (1998) 3652.
[30] M.W. Lufaso, P.M. Woodward, Acta Cryst. B 57 (2001) 725.
[31] M. O'Keeffe, B.G. Hyde, Acta Cryst. B 33 (1977) 3802.
[32] R.J. Bouchard, J.F. Weiher, J. Solid State Chem. 3 (1972) 80.
[33] J.W.G. Bos, J.P. Attfield, L.-Y. Jang, Phys. Rev. B 72 (2005) 014101.
[34] H.S. Jarrett, A.W. Sleight, H.H. Kung, J.L. Gilson, J. Appl. Phys. 51 (1980) 3916.
[35] M.A. Senaris-Rodriguez, J.B. Goodenough, J. Solid State Chem. 116 (1995) 224.
[36] R.D. Shannon, Acta Cryst. A 32 (1976) 751.
[37] K. Iwasaki, T. Ito, T. Nagasaki, Y. Arita, M. Yoshino, T. Matsui, J. Solid State Chem. 181 (2008) 3145.
[38] C.G.S. Pillai, A.M. George, Int. J. Thermophys. 4 (1983) 183.